[Supplementary Information]

Simultaneous Desalination and Selective Metal Recovery Enabled by Potential-regulated Electrochemical Ion Pumping

Longqian Xu,[1] Oluwatosin A Bello,[2] Shawon Sk Md Ali Zaker,[3] Bing Zhao,[1] Shihong Lin[1,4,5,6]*

[1] Department of Civil and Environmental Engineering, Rice University, Houston, TX, USA.

[2] Department of Civil and Environmental Engineering, Vanderbilt University, Nashville, TN, USA

[3] Department of Chemical and Biomolecular Engineering, Vanderbilt University, Nashville, TN, USA

[4] Department of Chemical and Biomolecular Engineering, Rice University, Houston, TX, USA.

[5] Rice Center for Membrane Excellence, Rice University, Houston, TX, USA.

[6] Rice WaTER Institute, Rice University, Houston, TX, USA.

Corresponding author email:

shihong.lin@rice.edu

Content

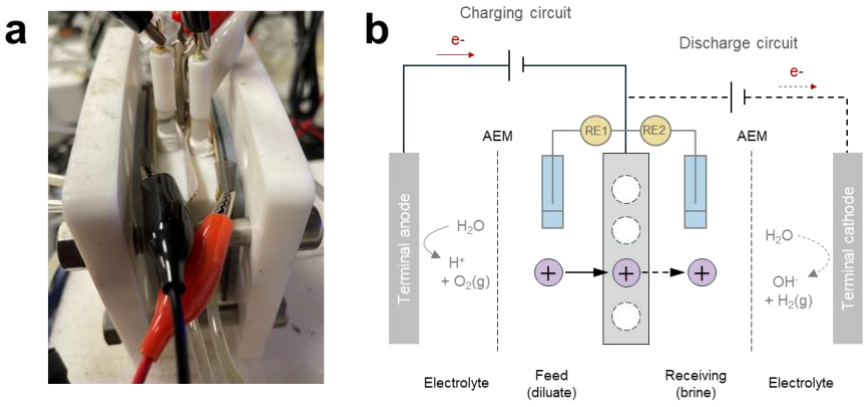

Supplementary Fig. 1. Configuration of the symmetric electrochemical ion pumping (s-EIP) system. a, Photograph of the s-EIP device equipped with a single cation shuttle electrode (CSE). **b**, Schematic of the electrical circuit design used to monitor the electrode potential of the CSE during switching between the charging and discharging circuits. Two Ag/AgCl reference electrodes (RE1 and RE2) were used to measure the electrode potential.

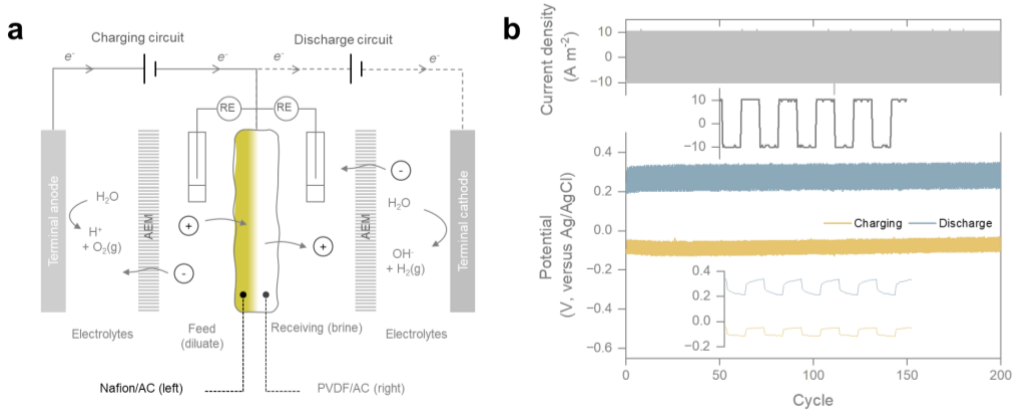

Supplementary Fig. 2. Effect of ion-exchange polymer coating on the electrode potential in the EIP system. a, Schematic illustration of an s-EIP cell with structurally asymmetric electrodes. The electrode facing the feed solution was coated with a cation-exchange polymer (Nafion + carbon), whereas the electrode facing the receiving solution used the conventional electrode formulation (PVDF + carbon). **b,** Evolution of electrode potential during repeated switching between the charging and discharging circuits. The upper panel shows the applied current density, and the lower panel shows the corresponding electrode potentials measured versus Ag/AgCl. Measurements were conducted in 50 mM NaCl electrolyte with a half-cycle duration of 5 s and a current density of 10 A m^{-2}.

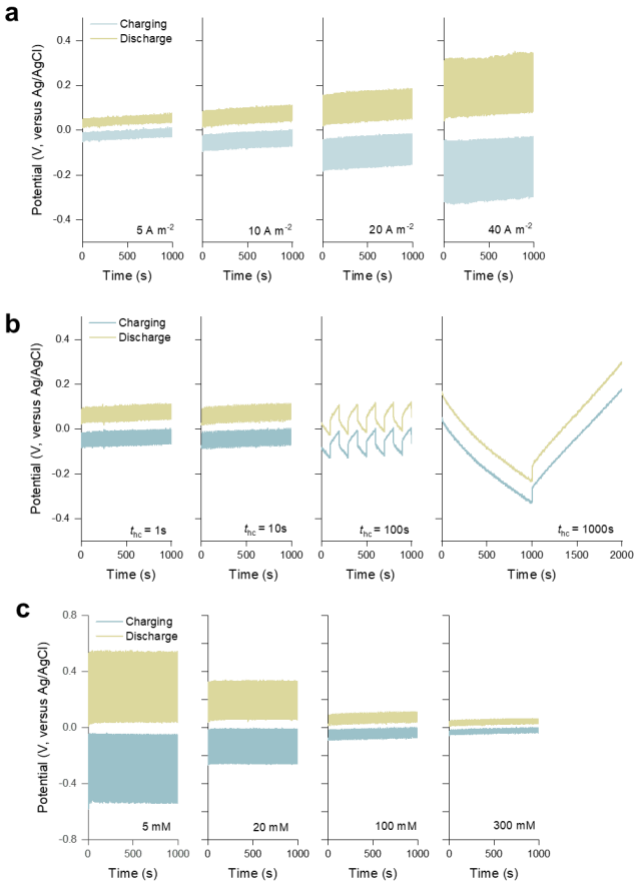

Supplementary Fig. 3. Effect of operating conditions on the potential of the cation shuttle electrode (CSE). a, Potential profiles of the CSE during charging and discharging at different current densities (5, 10, 20 and 40 A m^{-2}). **b,** Potential profiles of the CSE during charging and discharging at different half-cycle durations (1, 10, 100 and 1000 s). **c,** Potential profiles of the CSE during charging and discharging at different salt concentrations in the feed solution (5, 20, 100 and 300 mM).

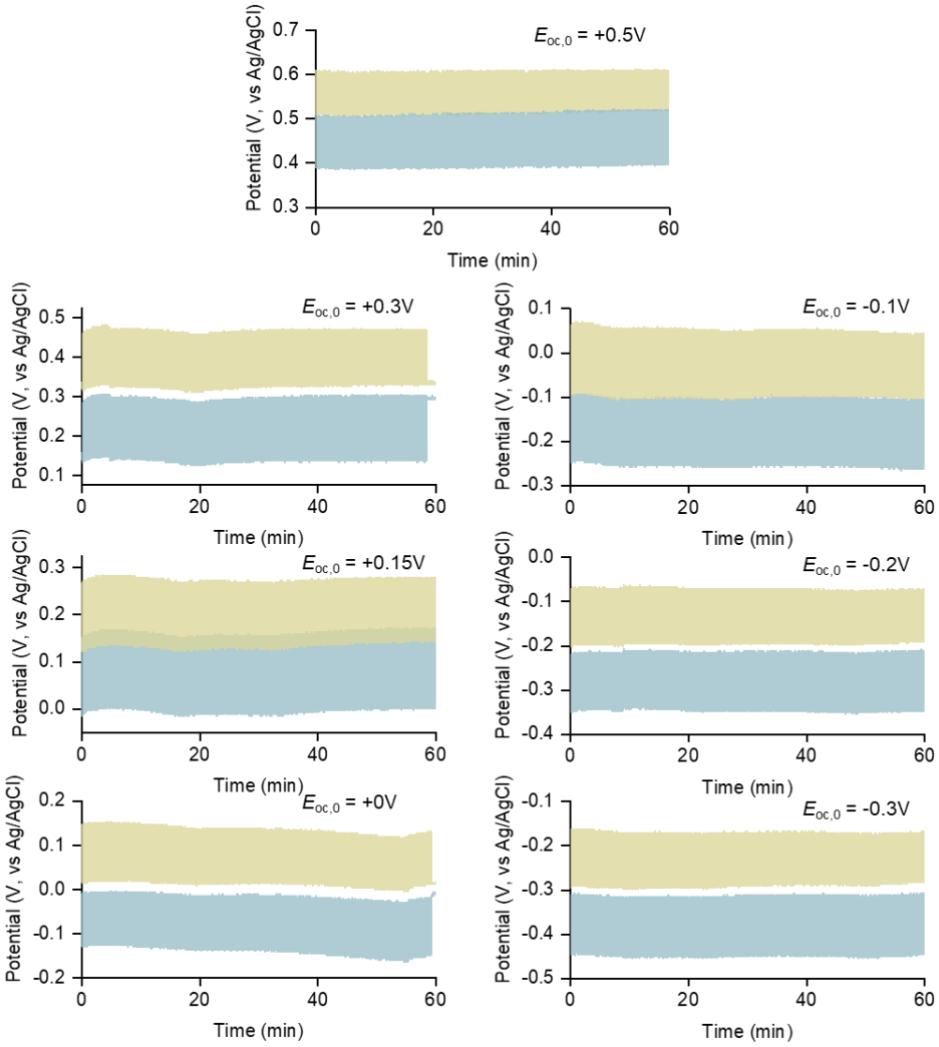

Supplementary Fig. 4. Potential profiles under different initial open-circuit potentials ($E_{oc,0}$). Potential profiles were recorded at initial $E_{oc,0}$ of +0.5, +0.3, +0.15, 0, –0.1, –0.2 and –0.3 V. The electrode potential was stabilized at different levels by tuning the time ratio between the charging and discharging half-cycles.

Supplementary Note 1: Estimation of the equilibrium potential of the Cu^{2+}/Cu couple

The equilibrium potential of the Cu^{2+}/Cu redox couple under the experimental electrolyte composition was estimated using the Nernst equation:

$$Cu^{2+} + 2e^- \rightleftharpoons Cu(s)$$

$$E = E^{\circ}_{Cu^{2+}/Cu} + \frac{0.05916}{2} \log\, a_{Cu^{2+}}$$

where $E^{\circ}_{Cu^{2+}/Cu}$ is the standard potential of the Cu^{2+}/Cu couple and $a_{Cu^{2+}}$ is the activity of free Cu^{2+}. Using $E^{\circ}_{Cu^{2+}/Cu} = 0.340\text{V}$ versus SHE and a total $CuCl_2$ concentration of 1 mM, the Cu^{2+} concentration is on the order of 10^{-3} M. Considering the background electrolyte composition (50 mM NaCl + 1 mM $CuCl_2$), the ionic strength is approximately 0.053 M, for which the activity coefficient of Cu^{2+} is estimated to be about 0.45. The activity of Cu^{2+} is therefore approximated as

$$a_{Cu^{2+}} \approx 0.45 \times 10^{-3} = 4.5 \times 10^{-4}$$

Substituting this value into the Nernst equation gives

$$E \approx 0.340 + \frac{0.05916}{2} \log(4.5 \times 10^{-4}) \approx 0.241 \text{ vs. SHE}$$

Because the reference electrode used in this work was Ag/AgCl (saturated KCl), with a potential of approximately 0.197 V versus SHE, the equilibrium potential on the Ag/AgCl scale is

$$E_{Cu2+/Cu} \approx 0.241 - 0.197 = 0.044\, V \text{ vs. Ag/AgCl}$$

therefore, the equilibrium potential of the Cu^{2+}/Cu redox couple under the present conditions was estimated to be approximately 0.04 V versus Ag/AgCl.

The Ag/AgCl reference electrode was positioned approximately 3–5 mm from the electrode surface. This distance does not affect the thermodynamic equilibrium potential itself, but under current flow it may contribute to a small uncompensated solution resistance.

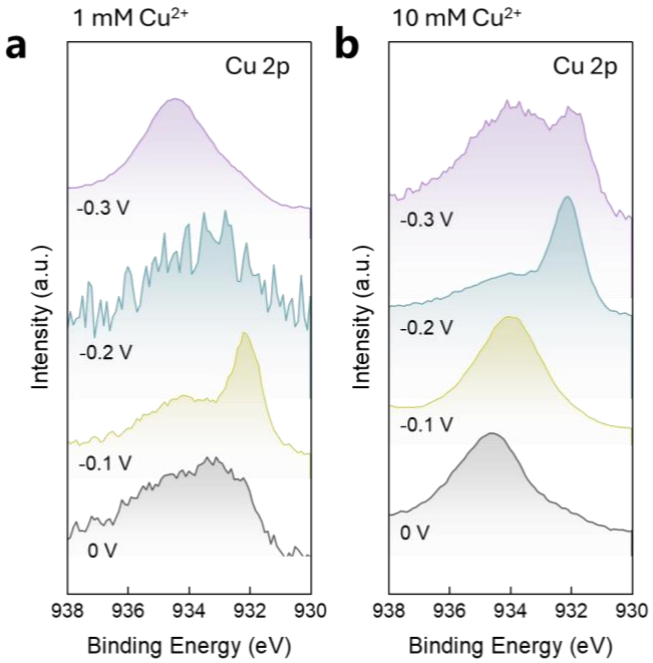

Supplementary Fig. 5. X-ray photoelectron spectroscopy (XPS) spectra of the deposits on the electrodes. a, Electrodes obtained under the low-Cu^{2+} condition (1 mM). **b**, Electrodes obtained under the high Cu^{2+} condition (10 mM).

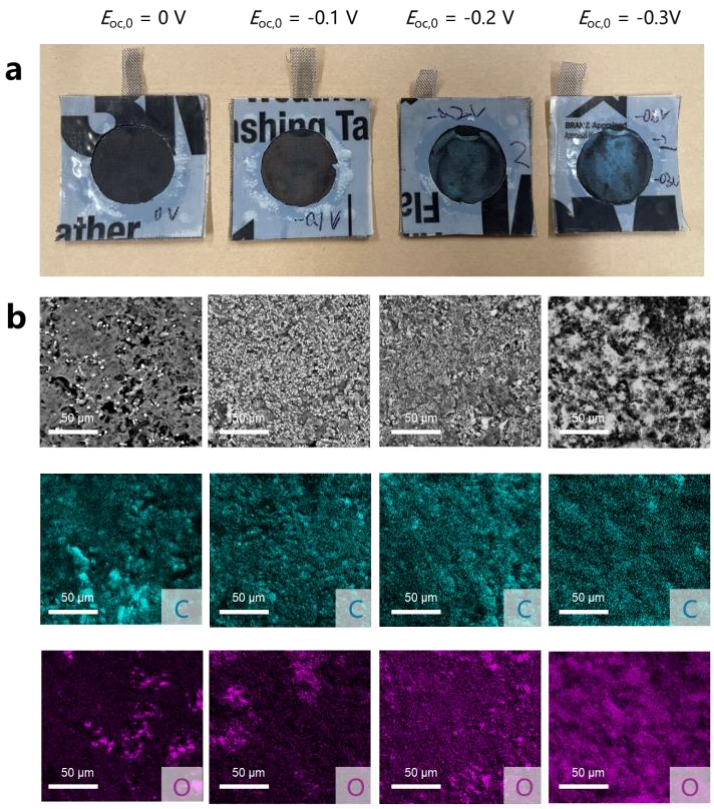

Supplementary Fig. 6. Surface morphology of the electrode under different potentials. a, Photographs of the electrode surfaces on the feed-solution side after operation at different $E_{\mathrm{oc},0}$. **b,** Scanning electron microscopy (SEM) images and corresponding energy-dispersive X-ray spectroscopy (EDS) elemental maps (C and O) of the electrode surfaces. All tests were conducted using a solution containing 50 mM NaCl and 1 mM $CuCl_2$.

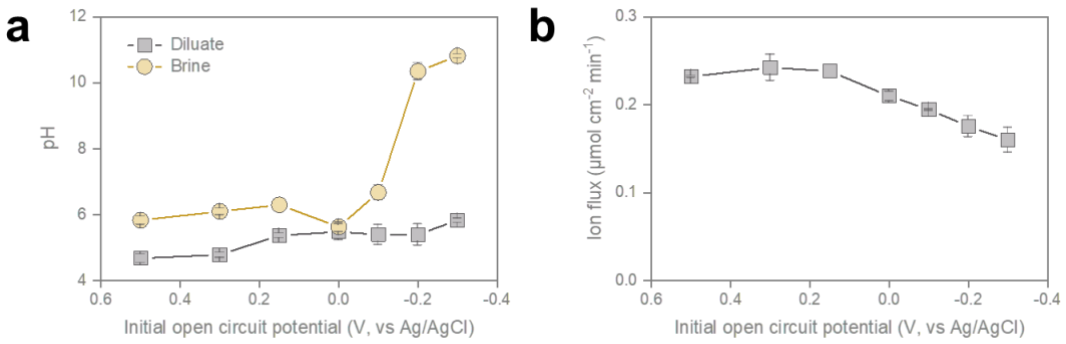

Supplementary Fig. 7. Effect of the initial open-circuit potential ($E_{oc,0}$) on the performance of the symmetric EIP (s-EIP). a, pH values of the diluate and brine streams at different $E_{oc,0}$. The pH of the diluate remains nearly constant over the examined potential range, indicating minimal parasitic reactions at the electrodes. In contrast, the brine pH increases markedly at more negative $E_{oc,0}$ values, which is attributed to hydroxide generation at the terminal cathode followed by OH^- transport across the anion-exchange membrane. **b**, Ion flux as a function of $E_{oc,0}$. The ion flux decreases when $E_{oc,0}$ becomes negative, indicating that a fraction of the charge is consumed by Cu^{2+} capture. The lower ion flux at negative $E_{oc,0}$ may also reflect enhanced self-discharge, which reduces the effective charge available for ion transport.

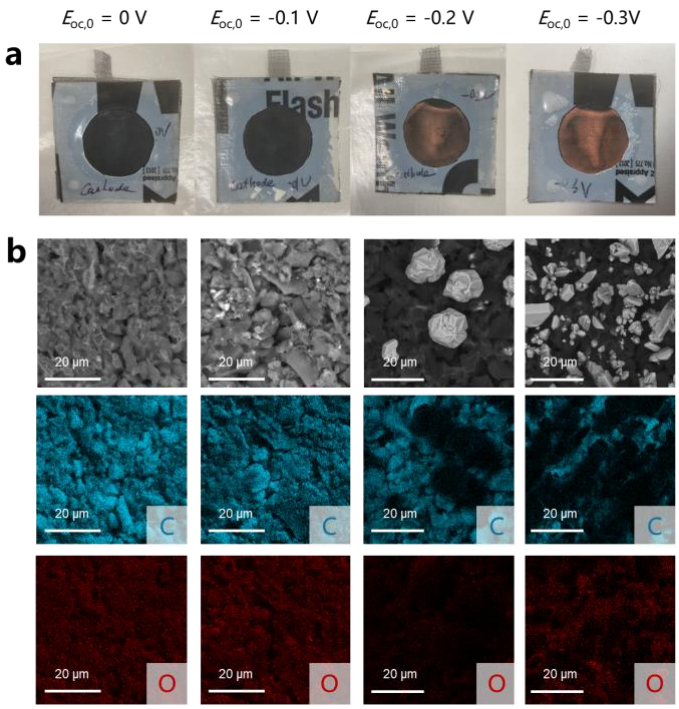

Supplementary Fig. 8. Surface morphology of the electrode under different potentials. a, Photographs of the electrode surfaces on the feed-solution side after operation at different $E_{oc,0}$. **b,** Scanning electron microscopy (SEM) images and corresponding energy-dispersive X-ray spectroscopy (EDS) elemental maps (C and O) of the electrode surfaces. All tests were conducted using a solution containing 500 mM NaCl and 10 mM $CuCl_2$.

Supplementary Note 2. Cu deposits release and electrode regeneration

Depending on the applied potential window, Cu^{2+} captured on the electrode can exist either as metallic Cu formed via electrochemical reduction or as Cu oxides/hydroxides formed through cathodically induced precipitation. Under highly negative potentials, the latter pathway becomes increasingly significant due to the generation of OH^- via water reduction at the electrode interface. Despite the different deposition mechanisms, the accumulated Cu species can be released and the electrode regenerated by reversing the electrode polarity and appropriately adjusting the electrode potential.

For deposits dominated by metallic Cu, regeneration can be achieved by increasing the electrode (anodic) potential above the Cu^{2+}/Cu equilibrium potential, thereby oxidizing Cu^0 back to soluble Cu^{2+}. For example, when the initial open-circuit potential ($E_{oc,0}$) is set to 0.5 V, the electrode potential during the discharge stage fluctuates within 0.5–0.8 V, which is sufficiently positive to drive Cu oxidation and dissolution. Four consecutive regeneration cycles were tested, demonstrating the high reversibility and stability of the Cu reduction–oxidation process (Supplementary Fig. 9a,c).

For deposits formed at more negative charging potentials, which primarily consist of Cu oxides/hydroxides, regeneration can be accomplished by further increasing the electrode potential to the range where water electrolysis occurs. In this regime, protons generated at the electrode interface can dissolve the deposited Cu hydroxides. Similarly, stable regeneration performance was observed over four consecutive cycles, confirming the robustness of this regeneration strategy (Supplementary Fig. 9b,d).

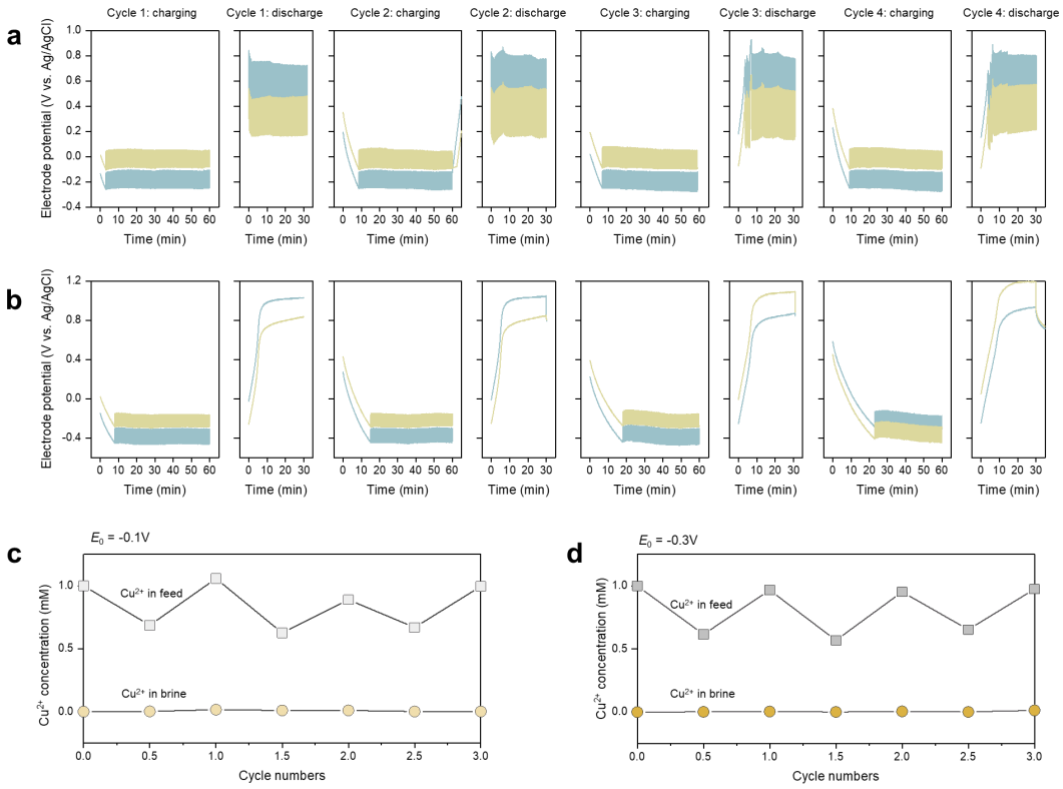

Supplementary Fig. 9. Electrode regeneration strategies for Cu-captured electrodes. a, Schematic of the regeneration strategy for electrodes bearing metallic Cu on the surface. Regeneration was achieved by shifting the electrode potential window to values above the Cu/Cu^{2+} redox potential, thereby promoting oxidation and release of deposited Cu. For example, Cu captured at Eoc,0 = −0.1 V could be released under a regeneration condition of $E_{oc,0}$ = +0.4 V. **b**, Schematic of the regeneration strategy for electrodes bearing $Cu(OH)_2$ deposits. In this case, regeneration was achieved by further increasing the electrode potential to induce water electrolysis. No circuit switching was applied during the discharge stage. **c,d**, Regeneration performance of the two strategies over four operating cycles. Experiments were conducted in an aqueous solution containing 50 mM NaCl and 1 mM $CuCl_2$. Each cycle consisted of a 60 min charging step at 10 A m^{-2} followed by a 30 min discharge step at 20 A m^{-2}.

Supplementary Note 3. Limitation of conventional electrosorption

Conventional electrosorption (ES), also known as capacitive deionization (CDI), typically operates under a full-capacity protocol, in which the electrodes are fully charged during the adsorption step and subsequently fully discharged during regeneration. As a result, each electrode undergoes a wide potential excursion during every charge–discharge cycle. When treating saline water containing heavy metal ions, such large potential windows can readily induce parasitic electrochemical reactions, leading to severe electrode scaling (Supplementary Fig. 10a). In addition, metal ions temporarily stored in the electrode through capacitive adsorption are released into the brine stream during discharge, generating secondary toxic effluents.

To illustrate these limitations, a conventional film electrode composed of activated carbon, carbon black, and PVDF (8:1:1 by mass) was tested in a CDI configuration. The electrode potential and Cu^{2+} behavior were monitored over four complete charge–discharge cycles. At a current density of 10 A m^{-2}, the electrode potential (starting as the cathode) decreased to approximately −0.5 V vs. Ag/AgCl within 1000 s during charging, and subsequently increased to about 0.7 V during discharge, corresponding to a potential window exceeding 1.2 V (Supplementary Fig. 10b).

Although the salt concentration in the feed solution decreased significantly after four cycles, the large negative potentials likely triggered Cu^{2+} reduction and/or cathodically induced precipitation, resulting in extensive Cu deposition on the electrode surface. Most of the deposited Cu could not be released during the discharge step and instead accumulated on the electrode as persistent scaling, which progressively increased with cycling (Supplementary Fig. 10c). Meanwhile, a smaller fraction of Cu was released into the brine stream during discharge, producing a toxic metal-containing waste stream.

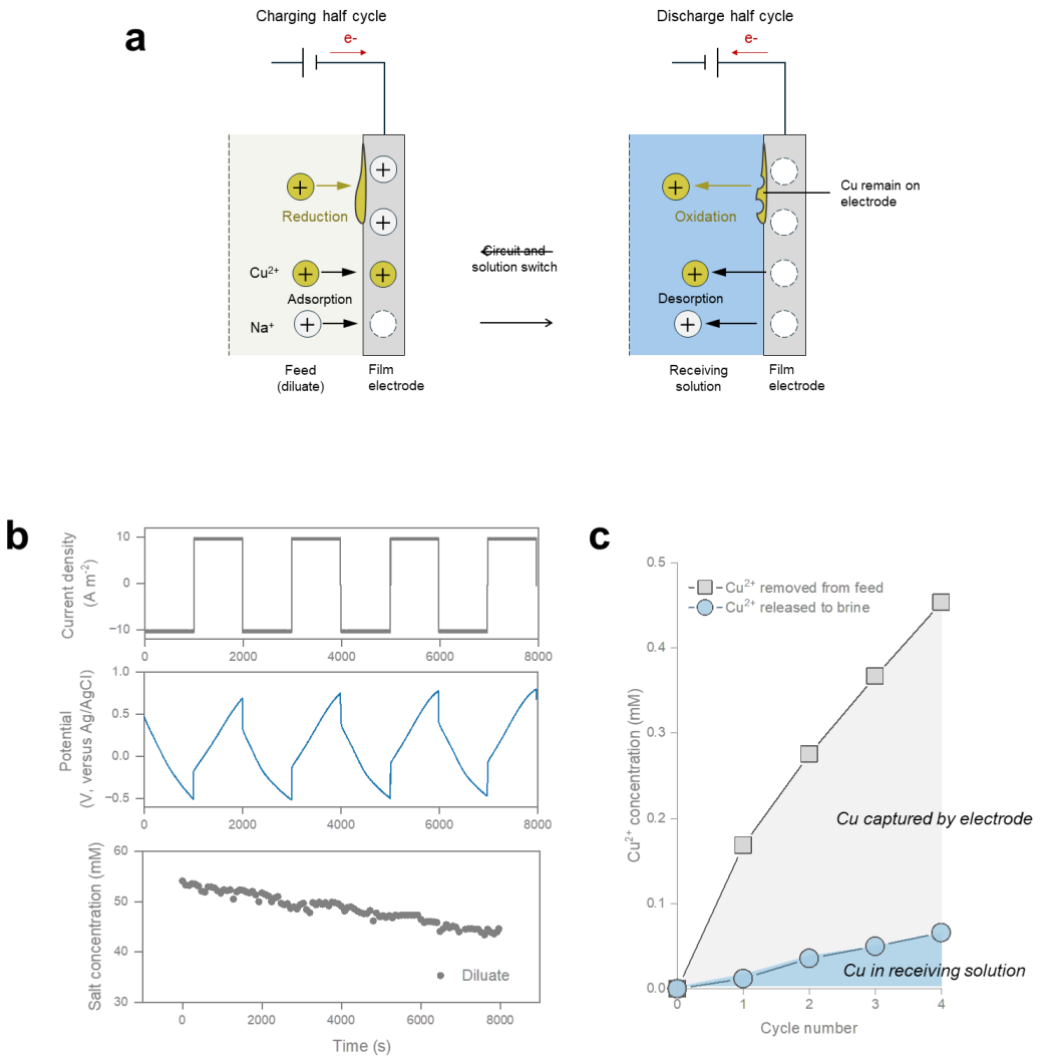

Supplementary Fig. 10. Separation performance of conventional electrosorption (ES). a, Schematic of Cu behavior during ES operation. **b**, Electrode potential and salt concentration profiles during four consecutive ES cycles. The upper panel shows the applied current density, the middle panel shows the electrode potential versus Ag/AgCl, and the lower panel shows the salt concentrations in the diluate and brine streams. **c**, Removal of Cu^{2+} from the feed solution and its release into the brine stream during ES operation. The grey shaded region highlights Cu^{2+} captured by the electrodes. The feed solution contained 50 mM NaCl and 1 mM $CuCl_2$, and a constant current density of 10 A m^{-2} was applied. Each ES cycle lasted 2000 s, with equal charging and discharging durations. Experiments were conducted using a capacitive deionization (CDI) cell equipped with a pair of activated carbon electrodes.

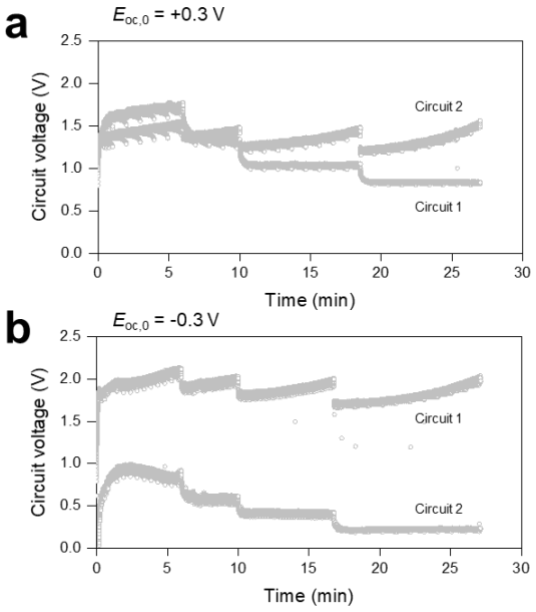

Supplementary Fig. 11. Circuit voltage profiles during EIP switching operation. a, Circuit voltage as a function of time under the high-potential operating condition (Eoc,0 = +0.3 V). **b**, Circuit voltage as a function of time under the low-potential operating condition (Eoc,0 = -0.3 V).

Supplementary Note 4. Construction of a multi-electrode symmetric EIP stack.

EIP cell can be constructed in two configurations depending on the type of electrodes employed: a symmetric EIP (s-EIP) and an asymmetric EIP (a-EIP). In s-EIP, all electrodes are of the same type, typically cation shuttle electrodes (CSEs), and adjacent electrodes are separated by an anion-exchange membrane (AEM). During operation, the CSE serving as the cathode stores cations, whereas the CSE serving as the anode releases cations (Supplementary Figure 12a). The AEM allows anions to migrate between the compartments to maintain charge balance. As the cycle proceeds, the cathodic potential gradually decreases while the anodic potential increases. However, when the symmetric configuration is used to regulate the electrode potential window, the duration of the charging half-cycle (t_{hc}^{c}) must be longer than that of the discharging half-cycle (t_{hc}^{d}) in order to compensate for self-discharge. This requirement contradicts the fundamental operation principle of the symmetric EIP, making it unsuitable as the basis for potential-window control.

In contrast, the asymmetric EIP configuration employs both CSEs and anion shuttle electrodes (ASEs), eliminating the need for ion-exchange membranes (Supplementary Figure 12b). Upon circuit activation, the CSE acting as the cathode stores cations, while the ASE acting as the anode stores anions. After switching the circuit, the CSE releases the stored cations and the ASE releases the stored anions. Because the charging and discharging half-cycles of each electrode pair can be controlled independently in time, the electrode potential can be tuned by adjusting the ratio between the charging and discharging durations (t_{hc}^{c}: t_{hc}^{d}). For example, if the potential window of the CSE is adjusted to a relatively low range, the ASE correspondingly operates at a higher potential.

To demonstrate the scalability and broader applicability of this concept, we constructed an asymmetric EIP stack comprising six ion-shuttle electrodes, with ASEs and CSEs arranged alternately, and two terminal electrodes positioned at the two ends of the stack (Supplementary Figure 12c). Specifically, circuit 1 consists of a terminal anode and a CSE, while circuit 6 consists of a terminal cathode and an ASE. The terminal electrodes balance charge through water electrolysis reactions. The intermediate circuits each contain one CSE and one ASE. Circuits 2 and 4 operate in the ion adsorption mode to generate a diluate stream, whereas circuits 3 and 5 operate in the ion desorption mode to generate a brine stream.

Before initiating selective metal capture using the EIP stack, the even-numbered circuits are first activated to lower the potentials of the two CSEs to the target values. After this preconditioning step, periodic circuit switching is initiated. To stabilize the potential window, the ratio between the charging and discharging half-cycles (t_{hc}^{c}: t_{hc}^{d}) must be appropriately adjusted. In practical desalination or separation processes, this ratio, together with the applied current density, may need to be tuned dynamically in response to changes in electrode behavior during operation.

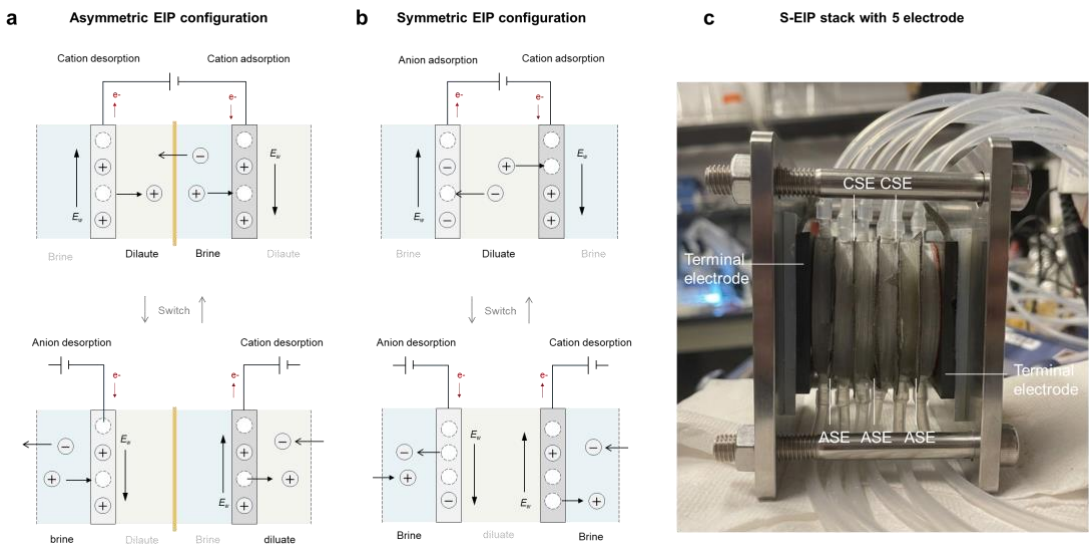

Supplementary Fig. 12. EIP configuration and stack design. a, Schematic of asymmetric EIP configuration. **b,** Symmetric EIP configuration. **c,** Photograph of the multi-electrode s-EIP stack.

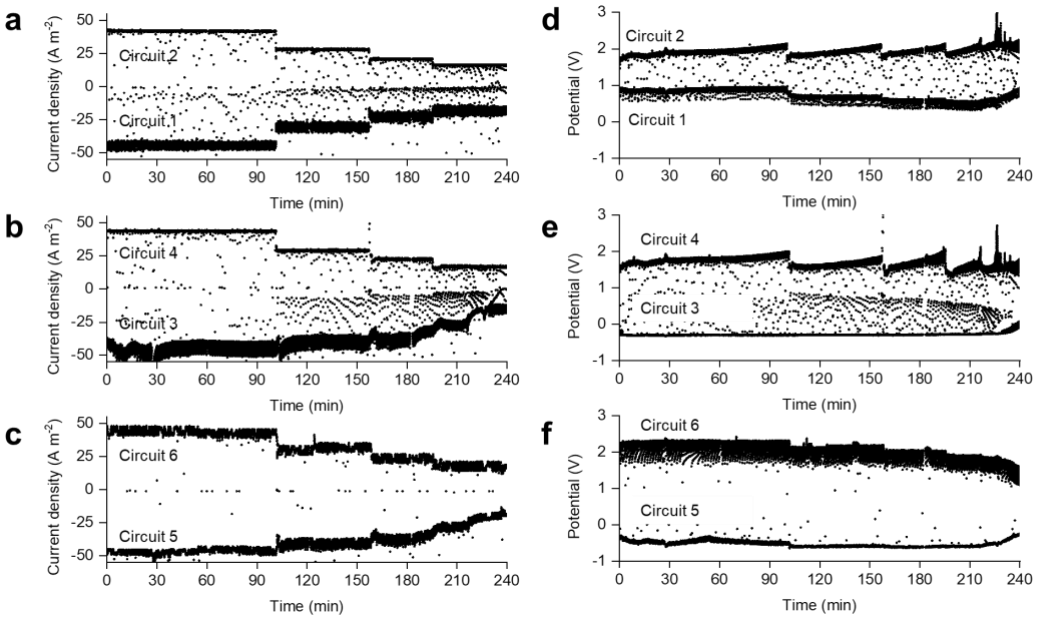

Supplementary Fig. 13. Current and voltage monitoring of the asymmetric EIP stack. a–c, Current profiles of the six circuits as a function of time during stack operation. **d–f,** Corresponding voltage profiles of the six circuits.

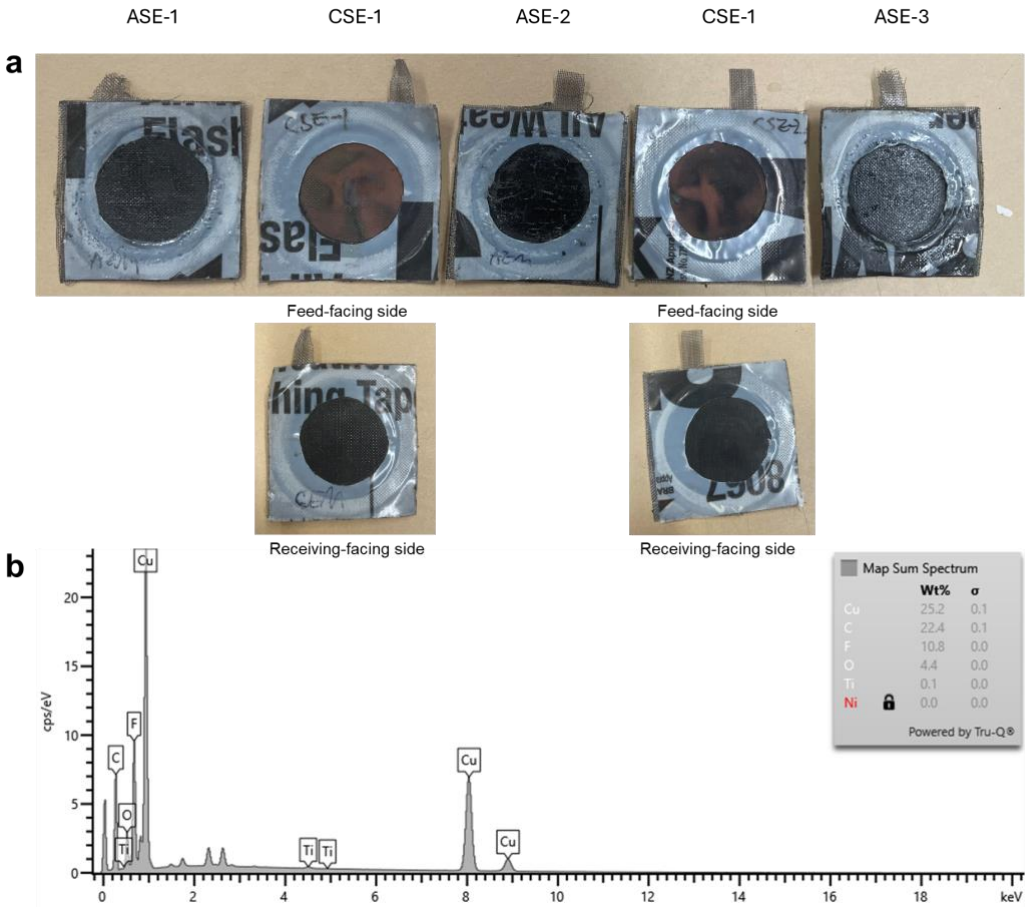

Supplementary Fig. 14. Asymmetric EIP stack for selective metal capture, electrode appearance, and product characterization. a, Photographs of the two CSEs and three ASEs after operation. **b,** EDS spectrum of the deposited product collected from the electrode surface.